J Mater Sci: Mater Electron (2016) 27:4326–4335
DOI 10.1007/s10854-016-4300-4

Electrical characterization of $SnSb_4S_7$ thin films by impedance spectroscopy

Imen Trabelsi[1] · Ahlem Jebali[1] · Mounir Kanzari[1,2]

Received: 24 July 2015 / Accepted: 6 January 2016 / Published online: 16 January 2016

Abstract SnSb4S7 thin films were deposited on glass substrate by vacuum thermal evaporation method. The effect of annealing on the structural and electrical properties of the SnSb4S7 thin films was investigated. The X-ray diffraction analysis revealed that the powder crystallized in monoclinic structure with a preferred orientation along $(\bar{2}1\bar{3})$ plane. SnSb4S7 thin films are polycrystalline in nature and the average grain size increases by increasing annealing temperature. Atomic force microscopy and scanning electron microscopy were used to characterize the surface morphology of the layers. Electrical properties have been investigated by ac impedance spectroscopy over a wide range of temperature up to 673 K starting from room temperature in the frequency range 5 Hz–13 MHz. The complex impedance plots display one semicircle with equivalent circuit functions as typical parallel RC. By increasing the temperature, the Impedance spectroscopy analysis shows that the resistance decreases from 10^7 Ω to 10^4 Ω. In addition, the analysis of conductivity indicates that both AC and DC conductivities of materials increase with increasing temperature The activation energy values calculated from DC conductivity and angular frequency relaxation are almost identical, indicating that the conduction mechanism was thermally activated and was assured by hopping between localized states.

✉ Imen Trabelsi
trabelsi.lpms@gmail.com

[1] Laboratoire de Photovoltaïque et Matériaux Semi-Conducteurs, Université Tunis El Manar, ENIT-, BP 37, Le belvédère, 1002 Tunis, Tunisia

[2] Institut Préparatoire aux Etudes d'Ingénieurs de Tunis Montfleury, Université de Tunis, Tunis, Tunisia

1 Introduction

In recent years, researchers paid particular attention to the sulfosalt semiconductors which had many applications field. Because of their excellent optical properties, sulfosalt materials are very attractive for a wide variety of technological applications such as thin film photovoltaic applications [1], phase change memory devices [2], thermoelectric energy conversion applications [3] and also it is promising to use sulfosalt in the sensor technologies field. $SnSb_4S_7$ is one member of the sulfosalt family $Sn_xSb_yS_z$ and is a very promising semiconductor that possesses important and advantageous properties for optoelectronic and solar cells applications [4–6].

Impedance spectroscopy (IS) is a valuable means for inquiring and has been extensively applied to study the frequency-dependent electrical properties of materials. The resistance and capacitance of crystallites and grain boundaries, which is frequency and temperature dependent, can be evaluated from IS spectra. This technique permits us to separate the real and imaginary part of the complex impedance and related parameters, and therefore provides information of the structure-properties correlation in the studied samples. We report in this work and for the first time at our knowledge a study of the electrical properties of the material $SnSb_4S_7$ by impedance spectroscopy. The objective is the understanding of electrical conduction mechanisms in this new semiconductor material. So, in the present work, $SnSb_4S_7$ thin films were deposited by vacuum thermal evaporation on no heated glass substrates after what they were annealed under nitrogen atmosphere at 423, 523 and 625 K during 1 h. Therefore, the annealed $SnSb_4S_7$ thin films were examined by the well-known impedance spectroscopy method to investigate the electrical properties and the conduction processes. The results of

the electrical properties were correlated with those of structural and morphological properties.

2 Experimental detail

The compound $SnSb_4S_7$ was synthesized by direct fusion of the component elements weighted in the stoichiometric proportions 1: 4: 7. The mixture was sealed in vacuum in a quartz tube. In order to avoid explosions due to sulfur vapor presses, the quartz tube was heated slowly (10 °C/h). A complete homogenization could be obtained by keeping the melt at 600 °C for 51 h.

The tube was then cooled at the rate 10 °C/h. Therefore cracking, due to thermal expansion of the melt on solidification, was avoided. The compound obtained is gray color [6]. X-ray diffraction of $SnSb_4S_7$ powder analysis showed that only the $SnSb_4S_7$ phase was present in the ingot. Crushed powder of this ingot was used as raw material for thin films deposition (see Fig. 1).

$SnSb_4S_7$ thin films were deposited by single source thermal evaporation from a Molybdenum boat onto no heated glass substrates under vacuum of 10^{-5} Torr. After what the as deposited thin films were annealed under nitrogen atmosphere at 423, 523 and 625 K during 1 h.

The structural properties of the evaporated thin films were determined by X-ray diffraction (XRD) using CuK_α radiation ($\lambda = 0.154056$ nm). Impedance measurement is made by the method of impedance spectroscopy with the HP4192A impedance analyzer over a wide range of temperature up to 673 K starting from room temperature in the frequency range 5 Hz–13 MHz. The measurements were performed using two-electrodes, which were painted on the two extremities of the sample using silver paste.

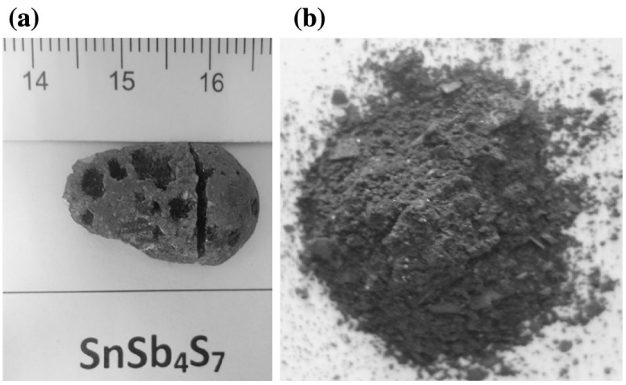

Fig. 1 **a** $SnSb_4S_7$ ingot, **b** $SnSb_4S_7$ powder

3 Results and discussion

3.1 Structural analysis

3.1.1 X-ray diffraction of $SnSb_4S_7$ powder

Figure 2 shows the X-ray diffraction patterns of our synthesized $SnSb_4S_7$ powder and the one taken from the reference (ICSD-169941) [7]. The concordance between both patterns confirms that only the phase $SnSb_4S_7$ exists with a privileged orientation along the $(\bar{2}1\bar{3})$ plane located at $2\theta = 31.5°$. We note that $SnSb_4S_7$ material crystallizes in the monoclinic structure [6].

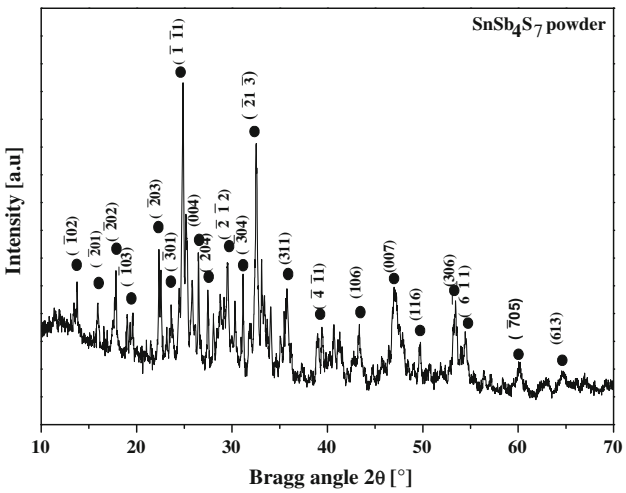

Fig. 2 X-ray diffraction patterns of the $SnSb_4S_7$ powder

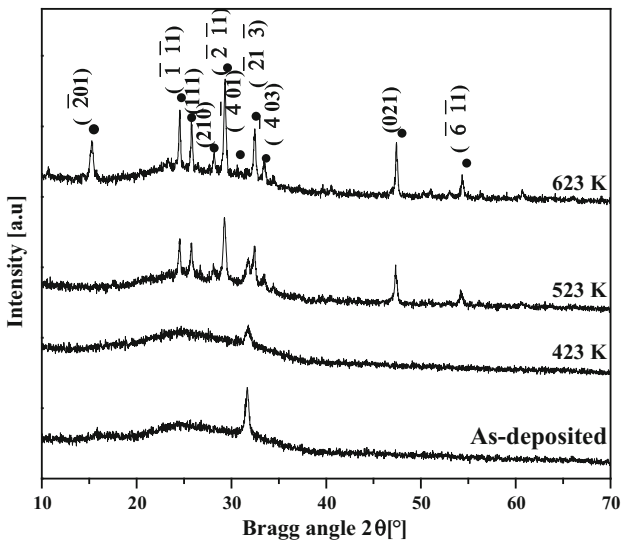

Fig. 3 X-ray diffraction patterns of $SnSb_4S_7$ thin films after annealing

3.1.2 X-ray diffraction of $SnSb_4S_7$ thin film: effect of annealing temperature under nitrogen atmosphere

Figure 3 shows XRD patterns of as-prepared and annealed $SnSb_4S_7$ thin films. All the diffraction peaks could be attributed to the monoclinic structure of $SnSb_4S_7$ (ICSD-169941). All the films show preferred orientation along the $(\bar{2}1\bar{3})$ plane. By increasing annealing temperature it is clear that more peaks appear which assigned to the $SnSb_4S_7$ phase.

Table 1 Structural and morphological properties of $SnSb_4S_7$ thin films at various annealing temperature

Annealing temperatures (K)	Grain size (nm) (Scherer's formula)	Crystallite size (nm) (instrumental broadening)	RMS (nm)
As-deposited	25.30	–	1.98
423	16.80	–	1.03
523	41.38	30.9	2.74
623	44.30	38.5	4.78

So, the appearance of these peaks confirms the enhancement of the crystallinity of the annealed films. Indeed, to confirm this, the crystallite size was calculated using the XRD patterns (see Table 1).

The crystallite size can be simply determined using the Debye–Scherrer formula [8] (Eq. 1):

$$D = \frac{0.9\lambda}{\beta_{size}\cos\theta} \quad (1)$$

where D is average crystallite dimension, λ is the wavelength of CuK_α radiation, β_{size} is the integral breadth of a Bragg peak located at 2θ corrected for the broadening caused by the instrumental setup of the diffraction experiment and θ is the diffraction angle of the peak. Peak broadening in X-ray or neutron powder diffraction can be attributed to one or more of the following sources: instrumental broadening, finite crystallite size, the presence of micro-strain and/or extended defects (stacking faults, micro-twinning, dislocations, etc.) [9, 10].

The total broadening β_t is given by the Eq. (2)

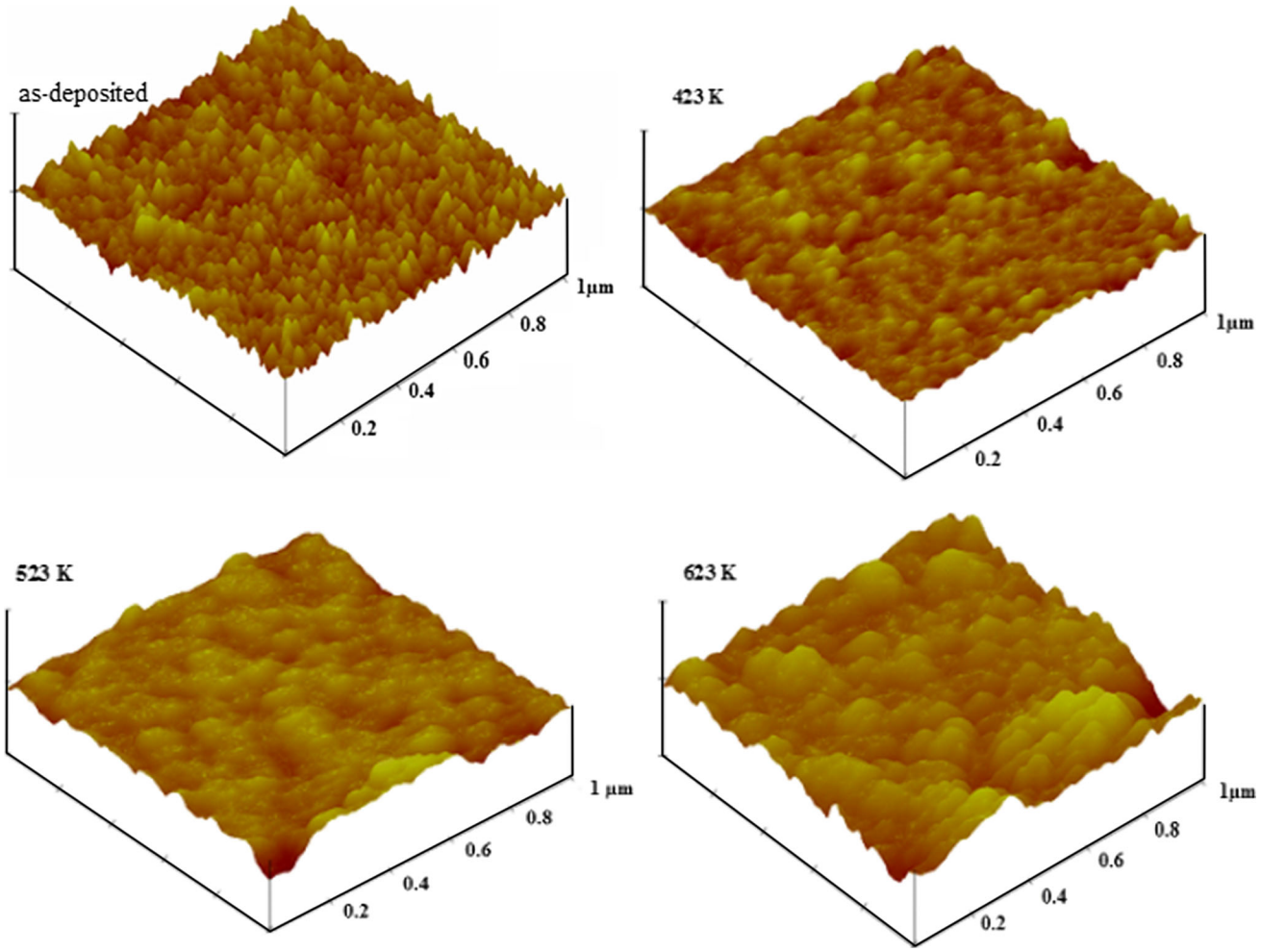

Fig. 4 3D-AFM images of $SnSb_4S_7$ thin films at different annealing temperature

$$\beta_t^2 \approx \beta_0^2 + \beta_{size}^2 + \{4\varepsilon \tan\theta\}^2 \quad (2)$$

$$(\beta_t^2 - \beta_0^2)\cos^2\theta = \left(\frac{0.9\lambda}{D}\right)^2 + \{4\varepsilon \sin\theta\}^2 \quad (3)$$

where ε is the strain and β_o the instrumental broadening ($\beta_o = 0.02°$). When we plot $(\beta_t^2 - \beta_0^2)\cos^2\theta$ versus $\sin^2\theta$ we get a straight line with slope $(4\varepsilon)^2$ and intercept $\left(\frac{0.9\lambda}{D}\right)^2$ (Eq. 3).

The average grain sizes of the layers were calculated using the principal diffraction. Table 1 summarizes all these values. We can note that the crystallite sizes were affected by annealing. So, we conclude that the crystallinity of the films was enhanced by increasing the annealing temperature.

3.2 Morphological properties

The morphology of SnSb4S7 thin films was investigated by atomic force microscopy (AFM, Taping mode) and scanning electron microscopy (SEM).

The surface morphology of SnSb4S7 thin films with and without annealing was analysed by atomic force microscope (AFM). Figure 4 shows the 3D AFM images taken in 0.1 μm × 0.1 μm area of the surface topography for the evaporated SnSb4S7 thin films. These images reveal that the surface morphology of the films changes by increasing the annealing temperature. It's clear that the as-deposited film is formed by very small crystallites and the annealed films show that the small crystallites have coalesced because of the annealing temperature, resulting in rougher surfaces with some additional big grains. The root mean square roughness (RMS) values of the films are given in Table 1

AFM analysis on the films annealed at different temperatures reveal that the surface roughness increases with the increase of the annealing temperature, suggesting an increase in crystallite size with temperature.

As expected, the surface morphology of the films changes when the annealing temperature increases, this is in a good agreement with the XRD results and confirms that the increase in annealing temperature changes the thin film structure.

SEM images have been obtained for samples at different annealing temperatures in order to study their effects on the

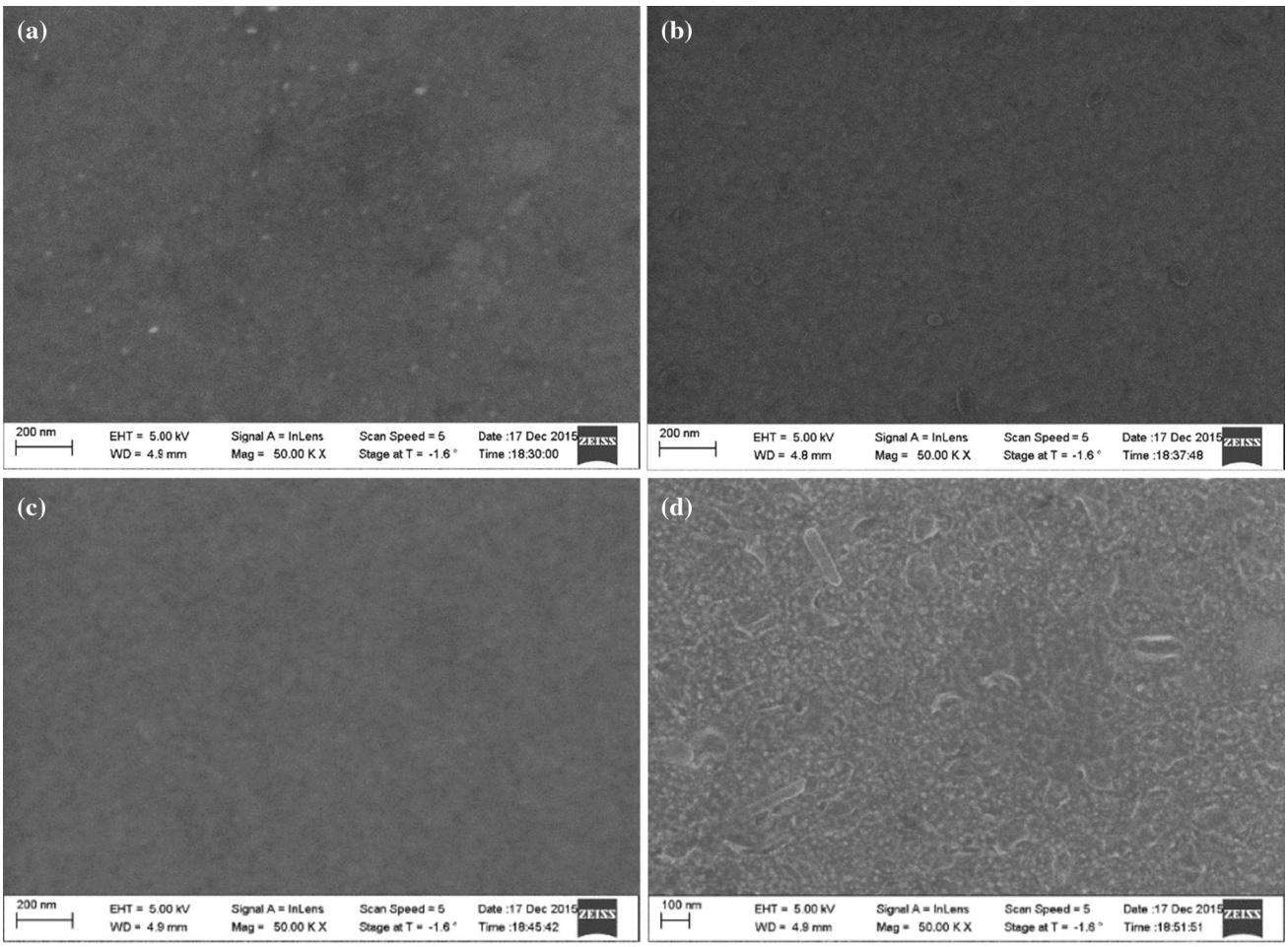

Fig. 5 SEM micrographsof $SnSb_4S_7$ thin films at different annealing temperature: **a** As-deposited, **b** 423 K, **c** 523 K, **d** 623 K

film surfaces. Figure 5 shows the micrographs of $SnSb_4S_7$ thin films. It is clear from the micrographs that all films surfaces are smooth and no isolated particles are observed. We noticed, for 623 K, a mixture of grains with different sizes and this morphology can explain the high values obtained for roughness. The surface is much more homogeneous than as-deposited thin film. For this case, the particles were distributed homogeneously on the surfaces and a difference in number and size with increasing annealing temperatures is observed. Once again, these results confirm those obtained by X-ray diffraction and by AFM.

3.3 Electrical properties

3.3.1 Impedance spectroscopy

Impedance spectroscopy technique consists in the application of sinusoidal voltage $v(t) = V_0 exp(j\omega t)$ to the sample and extract the value of current $i(t) = I_0 exp(j\omega t - \varphi)$. The complex impedance is defined as $Z = Z_0 ej\varphi$; Z_0 and φ allows defining imaginary and real part:

$$Re(Z) = Z' = Z_0 cos\varphi \quad (4)$$

$$Im(Z) = Z' = Z_0 sin\varphi \quad (5)$$

In general, in the case of non-isotropic material, the response of excitation process is shown as a pure resistance and a pure capacity in the case of an insulator. So, the response of the sample can be modeled as a parallel RC circuit (Debye model).

The spectra will present one or many semicircular arc that we can retrieve all characteristics as relaxation time, resistance and capacity. We should indicate that each semi-circle was an equivalent circuit treated as a combination of resistance and capacitance usually placed in parallel. The complex impedance of each arc is given by [11]

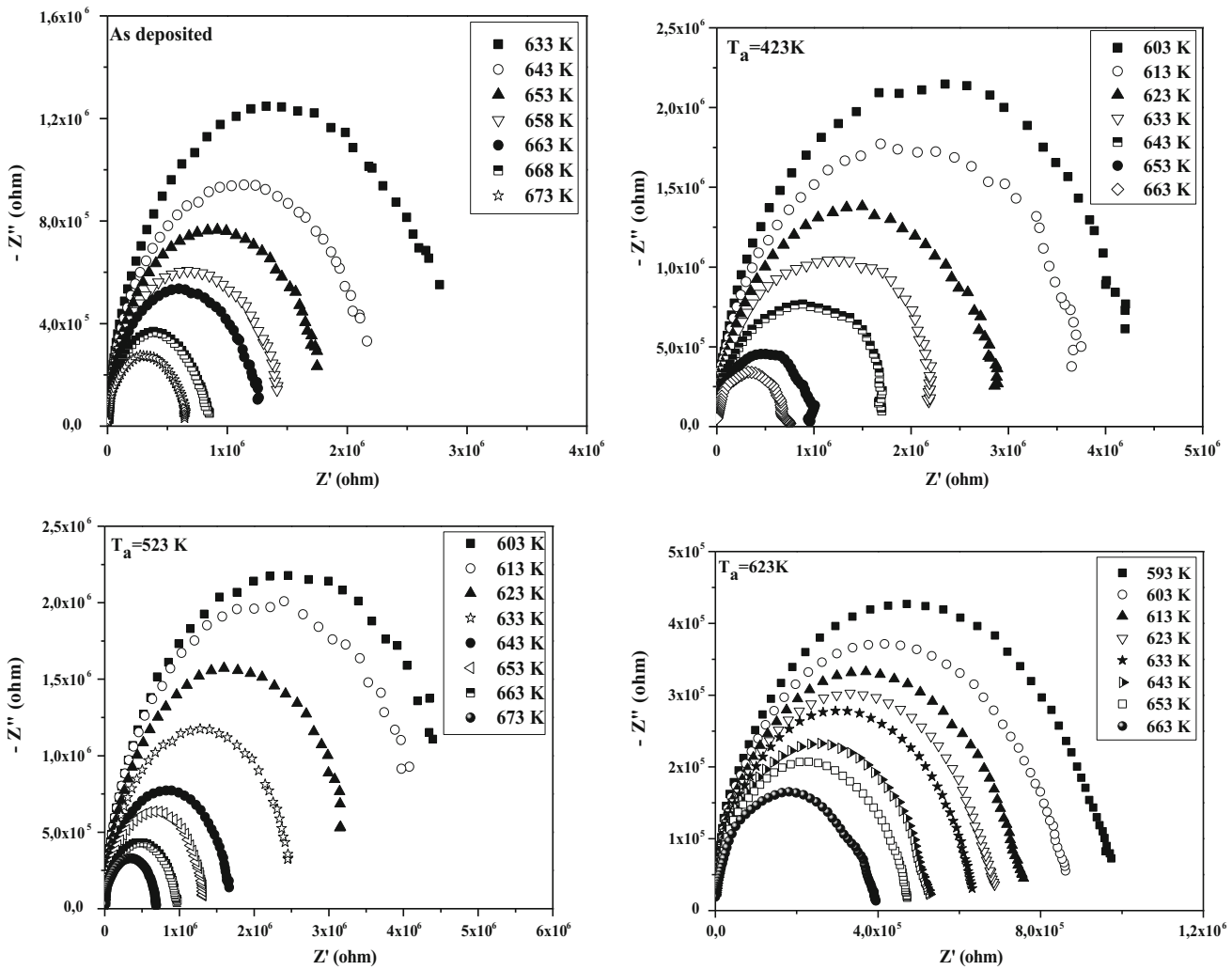

Fig. 6 Nyquist diagram of $SnSb_4S_7$ thin films at different annealing temperature

$$Z(\omega) = R/(1 + j\omega RC) \quad (6)$$

We remind that Impedance measurements were performed with the HP4192A impedance analyzer in the measurable impedance range from 5 Hz to 13 MHz with data taken at 20 points per decade. Real and imaginary parts were measured and displayed in the complex plane.

Figure 6 Shows the Nyquist diagrams de of annealed $SnSb_4S_7$ thin films. These spectra were obtained by plotting Z" as function of Z' in the temperature range for 593–673 K.

The obtained arcs present the response to excitatory electric fields applied to the sample and corresponds to intergranular polarization phenomenon intervening at higher frequencies. This combination is characterized by a time constant or characteristic relaxation time $\tau = RC = 1/\omega_m$ where ωm is the maximum angular pulsation. The top of arc was characterized by a maximum of angular frequency. We note that the maximum in Z" peak shifts to higher frequency with the temperature [12].

All spectra show a single semicircle slightly depressed indicating the single relaxation process. We note that their maximum shift to the higher frequencies as the temperature increases. Also, the diameter and the maximum of this semicircles decrease as the increasing of annealing temperature. These observations lead to the conclusion that the electrical conductivity is thermally activated well as the relaxation times distribution [13, 14]. As well, semi circles can indicate the homogeneity of evaporated $SnSb_4S_7$ thin films that is in good agreement with the morphological and structural results.

Tables 2, 3, 4, 5 shows the resistance values (R_p) of all samples. It is clear that the resistance decreases by increasing annealing temperature.

Figure 7 shows the dependence of imaginary part as angular frequency at various temperatures.

Therefore, the presence of peak frequencies shows an Arrhenius behavior which allows us to deduce the activation energy. Indeed, the relaxation time τ of these samples obeys to the well-known Arrhenius law [15]:

Table 2 Properties of $SnSb_4S_7$ thin films at characteristic frequency (As-deposited)

T (K)	R_p (ohm)	ln ω_m	Ln($T\sigma_{DC}$)	s
633	3.07E6	10.58	1.65	0.92
643	2.3E6	10.7	1.95	0.82
653	1.84E6	10.93	2.19	0.78
658	1.44E6	11.27	2.45	0.76
663	1.3E6	11.39	2.56	0.73
668	8.49E5	11.85	2.99	0.76
673	6.44E5	12.19	3.27	0.75

Table 3 Properties of $SnSb_4S_7$ thin films at characteristic frequency ($T_a = 423$ K)

T (°C)	Rp (ohm)	lnω_m	Ln($T\sigma_{DC}$)	s
603	4.37E6	10.81	1.25	1
613	3.76E6	11.16	1.42	0.97
623	2.96E6	11.27	1.68	0.87
633	2.26E6	11.39	1.96	0.88
643	1.73E6	11.73	2.24	0.82
653	9.88E5	12.42	2.82	0.83
663	7.44E5	12.77	3.12	0.85

Table 4 Properties of $SnSb_4S_7$ thin films at characteristic frequency ($T_a = 523$ K)

T(K)	Rp (ohm)	lnω_m	Ln($T\sigma_{DC}$)	s
603	4.75E6	10.12	1.5	1
613	4.29E6	10.24	1.62	0.92
623	3.28E6	10.58	1.88	0.89
633	2.53E6	10.81	2.23	0.91
643	1.69E6	11.16	2.57	0.79
653	1.32E6	11.5	2.86	0.84
663	9.88E5	11.85	3.17	0.81
673	6.82E5	12.19	3.55	0.80

Table 5 Properties of $SnSb_4S_7$ thin films at characteristic frequency ($T_a = 623$ K)

T (K)	Rp (ohm)	lnω_m	Ln($T\sigma_{DC}$)	s
593	1.00E6	11.73	2.94	0.83
603	8.85E5	11.85	3.08	0.81
613	7.68E5	11.96	3.24	0.79
623	6.67E5	12.08	3.40	0.80
633	6.37E5	12.19	3.46	0.76
643	5.32E5	12.31	3.66	0.80
653	4.79E5	12.42	3.78	0.80
663	4.01E5	12.65	3.97	0.78

$$\omega_m = \omega_0 exp(E_a/k_B T) \quad (7)$$

where ω_m is a constant. k_B is the Boltzmann constant and E_a is the activation energy. As shown in Fig. 5. the expression of $Ln(\omega_m) = f(1000/T)$ leads to a linear function, in good agreement with expression Eq. (7). E_a values were given in Table 6.

3.3.2 DC conductivity and temperature dependence

To identify the conduction process in the annealed in $SnSb_4S_7$ thin films, we can study the variation of DC conductivity versus temperature. The experimental data of

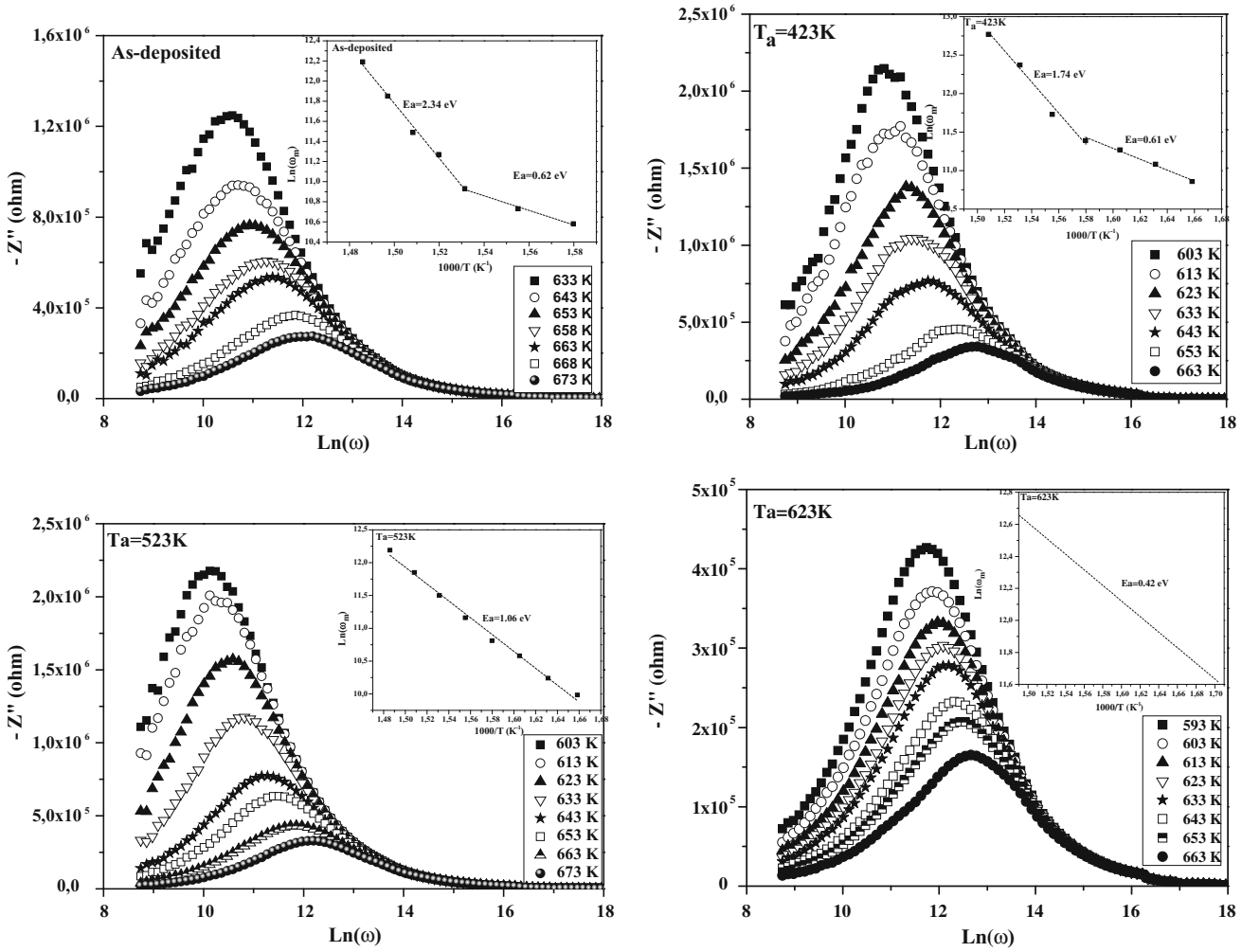

Fig. 7 Angular frequency dependence of Z'' at different annealing temperatures

Table 6 E_a values of $SnSb_4S_7$ thin films at various annealing temperature

Values obtained by	Maximum angular pulsation		Electrical conductivity	
Activation energy (eV)	E_{a1}	E_{a2}	E_{a1}	E_{a2}
As-deposited	2.34	0.62	2.03	0.96
423 K	1.74	0.61	1.46	0.78
523 K	1.06	–	1.03	–
623 K	0.42	–	0.48	–

the DC conductivity was analyzed using the following equations [13]:

$$\sigma_{DC} = (B/T)\, exp(E_a/k_B T) \tag{8}$$

where B is a constant independent of temperature T, k_B the Boltzmann constant and E_a is the activation energy.

The values of specific DC conductivity have been calculated (see Table 2) from the admittance data using relation

$$\sigma_{DC} = \frac{l}{s} \times \frac{1}{R_P} \tag{9}$$

where R_p is the intersection of the arc with real axis, l presents sample thickness and S the sample area under investigation [16].

Figure 8 shows the temperature dependence of DC conductivity. It's clear that DC conductivity is thermally activated and the values of the activation energy (E_a) have been estimated from the plots. As seen, the activation energy calculated from Eq. (8) is identical to the activation energy obtained from the angular relaxation frequency and E_a values decrease by increasing annealing temperature (see Table 6).

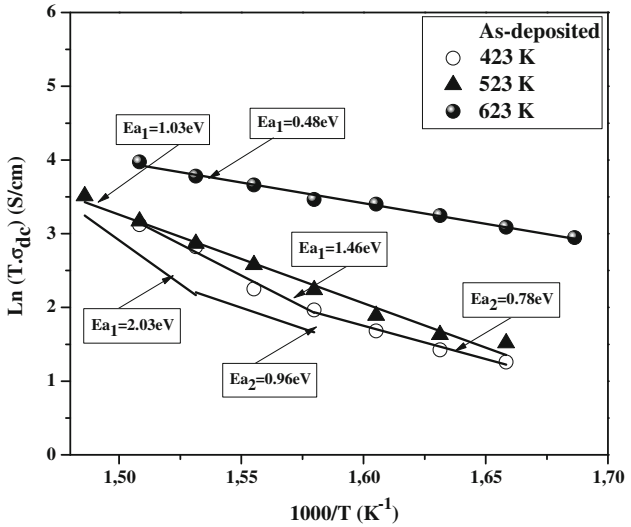

Fig. 8 Temperature dependence of DC conductivity of annealed $SnSb_4S_7$ thin films

In this case, the dominant transport mechanism insure by hopping conduction. Indeed, the localized charge carriers can jump from one site to other by thermal excitation where τ present the time of hopping [12–14].

3.3.3 *Dependence of AC conductivity on frequency and temperature*

AC conductivity measurements have been widely used to investigate the nature of defect centers in disordered systems since it is assumed that they are responsible for this conduction type [14, 17]. Generally, σ_{AC} in most of the cases has been observed to follow a universal power law [18] and dependence of AC conductivity on frequency is as given below

$$\sigma_{AC} = A\omega^s \tag{10}$$

where A is the temperature dependant constant and s (in general: $0 < s < 1$) is the frequency exponent.

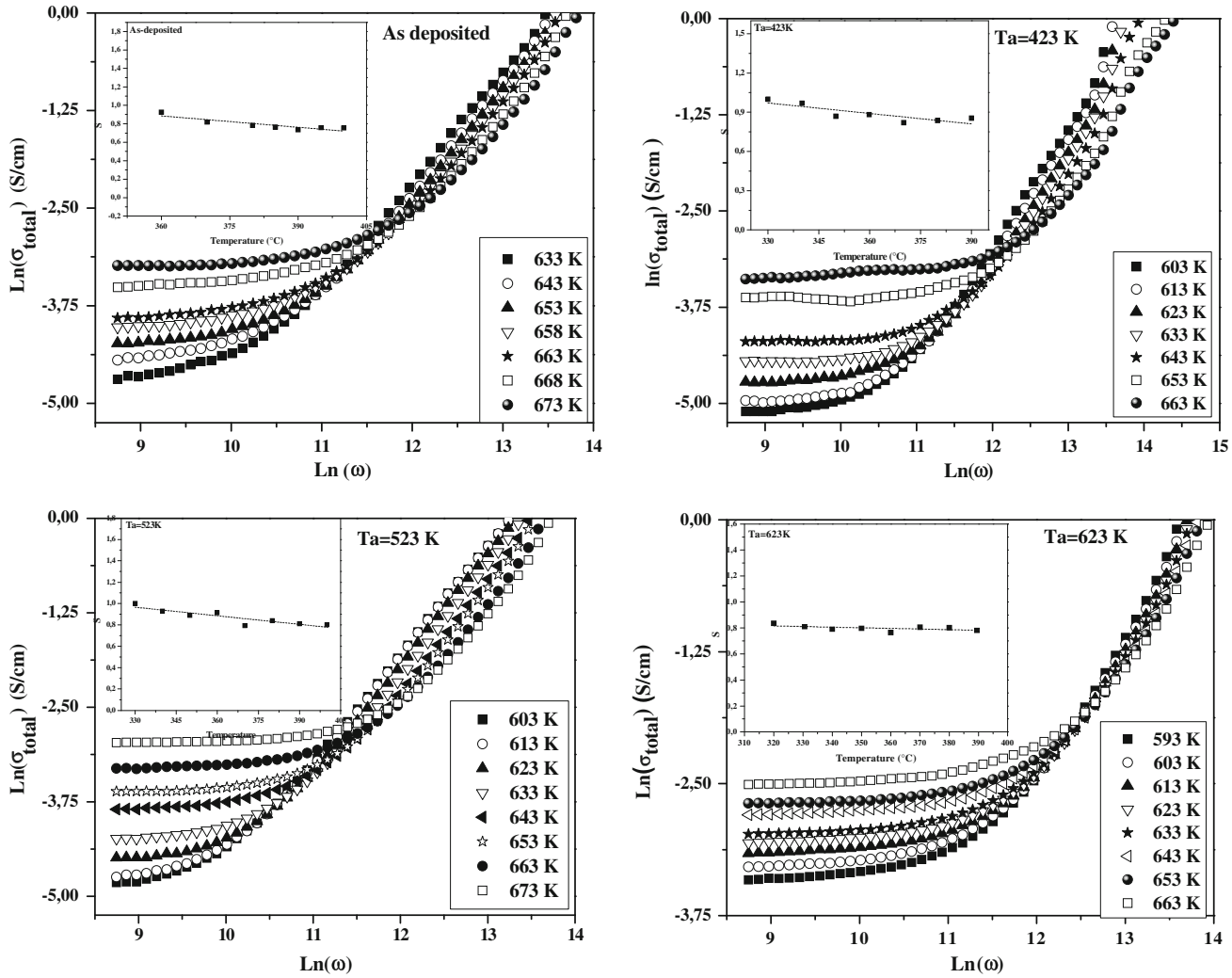

Fig. 9 Angular frequency dependence of total conductivity at different annealing temperature

The electrical conductivity $\sigma(\omega)$ of $SnSb_4S_7$ thin film at a particular temperature over a frequency range can be written in the combination of DC and AC part [19]:

$$\sigma(\omega) = \sigma_{DC} + A\omega^s \quad (11)$$

Figure 9 shows the dependence of conductivity as the function of angular frequency at different temperatures. It is clear that all plots present the same behavior. For all plots the conductivity increases with increasing of frequency showing a distinct change in slope from the critical maximum angular pulsation ω_m. Indeed, it is obvious that from Fig. 7 that for each plot, the linear region occurs from the maximum angular pulsation ω_m, which can be a sign of release of trapped charges in the disorder system. Whereas for the pulsations lower than ω_m the conductivity remains stable which may be due of free charge formation in the films [19]. On the other hand the slopes of the curves $\ln(\sigma_{AC})$ versus $\ln(\omega)$ were calculated at different temperatures and the slope has been designated as "*s*" [19, 20]. The interaction between all the charge species participating in the polarization process is characterized by the parameter "*s*" [19, 20]. The parameter *s* is used to describe the AC component contributing to the dispersive region [19, 20] (see Fig. 9; Tables 2, 3, 4, 5).

The values of "*s*" found in this work are less the unity and correlated to the charge carriers or extrinsic dipoles arising from the presence of defects and impurities in the film [21, 22]. Therefore, The AC conductivity shifts to higher frequency with the temperature which agrees with the observed shift of the relaxation frequency. It has been shown [23, 24] that the observed shift is originated from a thermally activated process. Then the conductivity dependence on frequency is an indication of hopping conduction at higher frequency between localized states [14, 17]. The temperature behavior of *s* could determine the conduction mechanism. In the CBH model that describes charge carrier hops between sites over the potential barrier separating them s decreases with the increment in temperature [25–28]. It is worth mentioning that the calculated values of s decrease with increasing rising temperature which is in good agreement with CBH model proposed by Elliot et al. [28, 29].

The results of the morphological properties indicate that as-deposited thin film was composed by very small crystallites containing grain boundaries. The free electrons passing through these grain boundaries at risk to make recombination [30]. With annealing treatment under nitrogen, crystallite size increases by increasing annealing temperature and the grain boundaries effect decrease. Indeed, the possibility of recombination decreases also and the number of charge carriers increases which promotes the conduction [31].

4 Conclusion

In conclusion, we have studied the effect of annealing under nitrogen atmosphere at 423, 523 and 625 K on structure and electrical behavior of $SnSb_4S_7$ thin films deposited on glass substrates by single source vacuum thermal evaporation method. All samples have a typical monoclinic structure and grown in a preferred orientation along the $(\bar{2}1\bar{3})$ plane located at $2\theta = 31.5°$. The crystallinity of the films was enhanced and the grain sizes were increased from 25 nm to 44 nm by increasing the annealing temperature. The morphological properties have been enhanced by annealing under nitrogen. Impedance spectroscopy analysis of $SnSb_4S_7$ thin film annealed under nitrogen atmosphere was performed in this work. The DC conductivity shows an increasing tendency with the increase of the annealing temperature. The results of this investigation reveal that the dielectric behaviour strongly depends on the annealing temperature. The activation energy obtained from both angular relaxation pulsation and DC conductivity suggest that the carrier transport mechanism is a hopping mechanism thermally activated in the band gap. Additional, the temperature dependent AC conductivity and the values of frequency exponent "*s*" suggest that correlated barrier hopping model (CBH) is the most suitable model to characterize the electrical conduction mechanism of the obtained $SnSb_4S_7$ thin films. So, all these electrical properties in addition of the optical ones of $SnSb_4S_7$ material show the interest of this material in optoelectronic applications [6].

References

1. H. Dittrich, A. Bieniok, U. Brendel, M. Grodzicki, D. Topa, Thin Solid Films **515**, 5745–5750 (2007)
2. M.Y. Versavel, J.A. Haber, Thin Solid Films **515**, 7171–7176 (2007)
3. A. Gassoumi, M. Kanzari, Physica E Low-Dimens. Syst. Nanostruct. **44**(1), 71–74 (2011)
4. D. Abdelkader, M. BenRabeh, N. Khemiri, M. Kanzari, Mater. Sci. Semicond. Process. **21**, 14–19 (2014)
5. N. Drissi, A. Gassoumi, H. Boughzala, J. Ouerfelli, M. Kanzari, J. Mol. Struct. **1047**, 61–65 (2013)
6. A. Jebali, N. Khemiri, F. Aousgi, M. Ben, Rabeh, M. Kanzari. Mater. Sci. Semicond. Process. **27**, 1057–1064 (2014)
7. ICSD-169941(Inorganic crystal structure database)
8. S.F. Bartram, *Handbook of X-Rays*, ed. by E.F. Kaelebe (McGraw-Hill, New York, 1967), Chap. 17
9. P. Karen, P.M. Woodward, J. Solid State Chem. **141**, 78–88 (1998)
10. T. Theivasanthi, M. Alagar, Nano Biomed. Eng. **4**(2), 58–65 (2012)
11. K. Prabakar, S.K. Narayandass, D. Mangalaraj, Mater. Chem. Phys. **78**, 809–815 (2003)

12. N. Kılınç, S. Öztürk, L. Arda, A. Altındal, Z.Z. Öztürk, J. Alloys Compd. **536**(25), 138–144 (2012)
13. B. Roy, S. Chakrabarty, M. Pal, A. Dutta, O. Mondal, Mater. Charact. **70**, 1–7 (2012)
14. A. Mhamdi, B. Ouni, A. Amlouk, K. Boubaker, M. Amlouk, J. Alloys Compd. **582**, 810–822 (2014)
15. T. Nagata, T. Shimura, A. Ashida, N. Fujimura, T. Ito. J. Cryst. Growth **237–239**(Part 1), 533–537 (2002)
16. V. Tudić, Engineering **6**, 449–461 (2014)
17. R. Ondo-Ndong, G. Ferblantier, F. Pascal-Delannoy, A. Boyer, A. Foucaran, Microelectron. J. **34**, 1087–1092 (2003)
18. A.K. Jonscher, *Dielectric Relaxation in Solids* (Chelsea Dielectric, London, 1983)
19. N.D. Sankır, E. Aydın, M. Sankır, Int. J. Electrochem. Sci. **9,** 3864–3875 (2014). www.electrochemsci.org
20. N.F. Mott, E.A. Davis, *Electronic Processes in Non-Crystalline Materials* (Clarendon Press, Oxford, 1979)
21. S.S.N. Bharadwaja, P. Victor, P. Venkateswarulu, S.B. Krupanidhi, Phys. Rev. B **65**, 174106 (2002)
22. P. Venkateswarlu, A. Laha, S.B. Krupanidhi, Thin Solid Films **474**, 1–9 (2005)
23. V. Biju, M.A. Khadar, J. Mater. Sci. **38**, 4055 (2003)
24. S. Kurien, J. Mathew, S. Sebastian, S.N. Potty, K.C. George, Mater. Chem. Phys. **98**, 470 (2006)
25. J.T. Gudmundsson, H.G. Svavarsson, S. Gudjonsson, H.P. Gislason, Phys. B **340**, 324 (2003)
26. T. Winie, A.K. Arof, Ionics **10**, 193 (2004)
27. M.A. Afifi, A.E. Bekheet, E.A. Elwahhab, H.E. Atyia, Vacuum **61**, 9 (2001)
28. A.A. Ebnalwaled, Int. J. Basic Appl. Sci. IJBAS-IJENS **11**(06), 194–207 (2011)
29. S.R. Elliott, Philos. Mag. **36**, 1291 (1977)
30. C. Magne, Thesis "Optimisation de couches d'oxyde nanostructurees pour applications aux cellules solaires a colorant" Ecole doctorale de chimie physique et analytique de Paris centre (ED388) 90-94 (2012). https://tel.archives-ouvertes.fr/tel-00833234/document
31. I. Trabelsi, N. Ben Mehrez, M. Kanzari, J. Mater. Sci.: Mater. Electron. **26**, 7763–7770 (2015)